J|A|C|S
ARTICLES
Published on Web 06/02/2007

Prototype Protein Assembly as Scaffold for Time-Resolved Fluoroimmuno Assays

Hannah N. Barnhill,[†] Stéphanie Claudel-Gillet,[‡] Raymond Ziessel,[‡] Loïc J. Charbonnière,*[,‡] and Qian Wang*[,†]

Contribution from the Department of Chemistry and Biochemistry and Nanocenter, University of South Carolina, 631 Sumter St., Columbia, South Carolina, and Laboratoire de Chimie Moléculaire, UMR 7509 au CNRS, ECPM, 25 rue Becquerel, 67087 Strasbourg Cedex 02, France

Received December 31, 2006; E-mail: wang@mail.chem.sc.edu; charbonn@chimie.u-strasbg.fr

Abstract: Turnip yellow mosaic virus (TYMV) is an icosahedral plant virus with an average diameter of 28 nm and can be isolated in gram quantities from turnip or Chinese cabbage inexpensively. In this study, it was selected as a prototype bionanoparticle for time-resolved fluoroimmuno assay (TRFIA). Two types of reactive amino acid residues were employed to anchor luminescent terbium complexes and biotin groups based on orthogonal chemical reactions. While terbium complexes were used as luminescent signaling groups, biotin motifs acted as a model ligand for protein binding. The bioconjugation results were confirmed by MS and Western blot analysis. Steady-state and time-resolved luminescence study of the dual-modified viruses demonstrated that the spectroscopic properties of the Tb complex are unperturbed by the labeling procedure. The dual-modified particle was probed by fluorescence resonance energy transfer (FRET) experiments using avidin labeled with an Alexa488 fluorophore, which bound to the biotin on the surface of the particle, as an energy acceptor, and terbium complexes as an energy donor. The emission and excitation spectra of the dual-labeled TYMV particle displayed residual virus fluorescence and Tb luminescence upon ligand-centered excitation. The Tb luminescence lifetime was 1.62 ms and could be effectively fitted with a single-exponential behavior. In the TRFIA, an efficient transfer of 66% was observed, and the calculation using the Förster radius of 41 Å allowed for an estimation of the average donor−acceptor distance of 36 Å. Our studies show that the two reactive sites can communicate with each other on the surface of a nanoscale biological assembly. In particular, the ligand−receptor binding (biotin and avidin in this paper) was not interfered with when anchored to the surface of TYMV. Therefore, as a prototype of polyvalent bionanoparticles, TYMV can be used as scaffold for sensor development with TRFIA.

1. Introduction

Viruses and virus-like particles (VLPs) have emerged over recent years as promising building blocks for chemical reactions and materials syntheses.[1−7] These bioinspired systems form monodispersed units that are highly amenable through genetic and chemical modifications. As nanoscale assemblies, viruses have sophisticated yet highly ordered structural features, which, in many cases, have been carefully characterized by modern structural biological methods, in particular, by X-ray crystallography and high-resolution electron microscopy. Therefore, viruses and VLPs offer a unique scaffold where functional motifs can be programmed on their coat proteins (termed as capsids) precisely at subnanometer scale via bioconjugation or supramolecular recognition,[5,8] which is a big advantage over synthetic nanoparticles.

Taking advantage of the defined structural morphology of viruses and the surface binding properties toward metal ion or metal oxides, viruses have been used as templates or reaction vessels for the syntheses of micro- or nanoscale inorganic materials. For example, semiconductive or conductive nanowires were prepared with rodlike tobacco mosaic virus (TMV) as template,[2,7,9−14] and spherical nanoparticles were produced using the hollow protein shell of icosahedral cowpea chlorotic mottle virus (CCMV) as a nanoreactor.[4,15] With genetically modified filamentous bacteriophage M13 as templates, inorganic, organic,

[†] University of South Carolina.
[‡] Laboratoire de Chimie Moléculaire, UMR 7509 au CNRS.

(1) Lee, L. A.; Wang, Q. *Nanomedicine* **2006**, *2*, 137.
(2) Douglas, T.; Young, M. *Adv. Mater.* **1999**, *11*, 679.
(3) Douglas, T.; Young, M. *Science* **2006**, *312*, 873.
(4) Douglas, T.; Young, M. *Nature* **1998**, *393*, 152.
(5) Wang, Q.; Lin, T.; Tang, L.; Johnson, J. E.; Finn, M. G. *Angew. Chem., Int. Ed.* **2002**, *41*, 459.
(6) Russell, J. T.; et al. *Angew. Chem., Int. Ed.* **2005**, *44*, 2420.
(7) Flynn, C. E.; Lee, S.-W.; Peelle, B. R.; Belcher, A. M. *Acta Mater.* **2003**, *51*, 5867.
(8) Mao, C.; Solis, D. J.; Reiss, B. D.; Kottmann, S. T.; Sweeney, R. Y.; Hayhurst, A.; Georgiou, G.; Iverson, B.; Belcher, A. M. *Science* **2004**, *303*, 213.
(9) Royston, E.; Lee, S. Y.; Culver, J. N.; Harris, M. T. *J. Colloid. Interface. Sci.* **2006**, *298*, 706.
(10) Lee, S. Y.; Choi, J. W.; Royston, E.; Janes, D. B.; Culver, J. N.; Harris, M. T. *J. Nanosci. Nanotechnol.* **2006**, *6*, 974.
(11) Slocik, J. M.; Naik, R. R.; Stone, M. O.; Wright, D. W. *J. Mater. Chem.* **2005**, *15*, 749.
(12) Fonoberov, V. A.; Balandin, A. A. *Nano Lett.* **2005**, *5*, 1920.
(13) Dujardin, E.; Peet, C.; Stubbs, G.; Culver, J. N.; Mann, S. *Nano Lett.* **2003**, *3*, 413.
(14) Fowler, C. E.; Shenton, W.; Stubbs, G.; Mann, S. *Adv. Mater.* **2001**, *13*, 1266.

and biological nanosized materials have been aligned into nanowires,[8,16] nanorings,[17] nanofibers,[18] films,[19,20] and other nanostructures.[21−23] Along with the emerging interests in using viruses and VLPs for drug delivery and other biomedical applications,[1,24−26] cowpea mosaic virus (CPMV) was the first virus to be demonstrated as a robust platform for conjugation with a variety of molecules, including fluorescent dyes,[5,27−29] quantum dots,[30] polymers,[31,32] stilbene derivatives,[29] biotin,[27,28] DNA,[33] peptides and proteins,[34−36] and carbohydrates.[32,37] Following CPMV, the chemical reactivities of many other viruses have been studied, including CCMV,[38] *Nudaurelia capensis omega* virus,[39] TMV,[40] and bacteriophage MS2.[41]

In addition, it is possible to engineer multiple orthogonal reactive sites on the viral capsid based on conventional bioconjugation techniques or newly developed chemistry.[5,40−43] Therefore, both signaling moieties (like fluorescent or magnetic molecules) and biological recognition motifs (such as haptens, antibodies, oligonucleotides, ligands, receptors, or chemical sensors) can be attached simultaneously on the viral capsids, which lead to possible nanosized probes for bioimaging or sensing. Recently it has been shown by Soto et al. that fluorescent dyes can be anchored on CPMV with controlled distance which prevented the formation of nonfluorescent dimers and subsequent quenching and afforded highly fluorescent viral nanoparticles.[44] Such kind of engineered viral particles can be used as probes in microarray-based genotyping assays and sandwich immunoassays with improved sensitivities.[36,44] In this paper, we present a prototype nanoprobe for time-resolved fluoroimmuno assays (TRFIA), which took advantage of the chemistry for orthogonal modifications, the high local concentration of binding and signaling motifs, and the symmetrical distribution of the reactive sites of the icosahedral plant virus. In particular, we aim to answer one fundamental question related to viral particle-based bioassays: whether the binding activities of ligands to protein receptors will be the same upon conjugation to viral capsids when compared with that of ligands in solution.

The icosahedral turnip yellow mosaic virus (TYMV) was employed in this study. As a member of the tymovirus group, TYMV is a plant virus with an average diameter of 28 nm and made of a single-stranded RNA of 1.9×10^6 Da and 180 chemically identical protein subunits of 20 133 Da. The subunits arrange into 60 trimeric asymmetric units loosely assembled in a $T = 3$ icosahedral symmetry as depicted in Figure 1.[45−47] The structure of TYMV has been exclusively studied by X-ray crystallographic analysis[45,46] and electron microscopy using negative staining.[48] It can be isolated from either the turnip or Chinese cabbage in gram quantities. In comparison with other plant viruses, TYMV has some unique advantages in chemistry, biomedical applications, and materials development. First, empty capsids can be isolated naturally from the host plant or generated artificially by treating under pressure,[49] basic environment,[50] or repeating freeze−thaw process.[51] Furthermore, some of these methods result in a hole in the otherwise intact capsid, which may provide a route for the introduction of useful materials such as quantum dots or drugs and opens the possibility of interior modification of the capsid. In addition, TYMV is stable from 4 °C to room temperature for months and 60 °C for several hours. It can stand for a wide pH range (4−10), up to 50% organic solvent, and a variety of reaction conditions. Finally, the capsid of TYMV represents a very rigid spherical assembly; therefore, we can predict the conformation of the coat proteins and attached molecules based on the X-ray structural data.[46]

A recently developed luminescent terbium complex (herein referred to as Tb**L**) was used as the signaling moiety.[52] The Tb**L** complex is highly luminescent, with high quantum yield in aqueous solutions (31%) and a long luminescence lifetime (1.5 ms). Tb**L** has also been shown to be an excellent donor for fluorescence resonance energy transfer (FRET) interactions, allowing for energy transfer where conventional organic fluorophores failed.[53] The use of such an energy donor with a long-lived excited state also permits a temporal discrimination of the energy transfer process, which eliminates the spurious fluorescence signals and increases the detection sensitivity.[54] The FRET communication between Tb**L** and fluorescently

(15) Douglas, T.; Strable, E.; Willits, D.; Aitouchen, A.; Libera, M.; Young, M. *Adv. Mater.* **2002**, *14*, 405.
(16) Mao, C.; Flynn, C. E.; Hayhurst, A.; Sweeney, R.; Qi, J.; Georgiou, G.; Iverson, B.; Belcher, A. M. *Proc. Natl. Acad. Sci. U.S.A.* **2003**, *100*, 6946.
(17) Nam, K. T.; Peelle, B. R.; Lee, S.-W.; Belcher, A. M. *Nano Lett.* **2004**, *4*, 23.
(18) Lee, S.-W.; Belcher, A. M. *Nano Lett.* **2004**, *4*, 387.
(19) Lee, S.-W.; Wood, B. M.; Belcher, A. M. *Langmuir* **2003**, *19*, 1592.
(20) Lee, S.-W.; Mao, C.; Flynn, C. E.; Belcher, A. M. *Science* **2002**, *296*, 892.
(21) Lee, S.-W.; Lee, S. K.; Belcher, A. M. *Adv. Mater.* **2003**, *15*, 689.
(22) Flynn, C. E.; Mao, C.; Hayhurst, A.; Williams, J. L.; Georgiou, G.; Iverson, B.; Belcher, A. M. *J. Mater. Chem.* **2003**, *13*, 2414.
(23) Reiss, B. D.; Mao, C.; Solis, D. J.; Ryan, K. S.; Thomson, T.; Belcher, A. M. *Nano Lett.* **2004**, *4*, 1127.
(24) Khor, I. W.; Lin, T.; Langedijk, J. P. M.; Johnson, J. E.; Manchester, M. *J. Virol.* **2002**, *76*, 4412.
(25) Rae, C. S.; Wei Khor, I.; Wang, Q.; Destito, G.; Gonzalez, M. J.; Singh, P.; Thomas, D. M.; Estrada, M. N.; Powell, E.; Finn, M. G.; Manchester, M. *Virology* **2005**, *343*, 224.
(26) Singh, P.; Gonzalez, M. J.; Manchester, M. *Drug Dev. Res.* **2006**, *67*, 23.
(27) Wang, Q.; Kaltgrad, E.; Lin, T.; Johnson, J. E.; Finn, M. G. *Chem. Biol.* **2002**, *9*, 805.
(28) Wang, Q.; Lin, T.; Johnson, J. E.; Finn, M. G. *Chem. Biol.* **2002**, *9*, 813.
(29) Wang, Q.; Raja, K. S.; Janda, K. D.; Lin, T.; Finn, M. G. *Bioconjugate Chem.* **2003**, *14*, 38.
(30) Medintz, I. L.; Sapsford, K. E.; Konnert, J. H.; Chatterji, A.; Lin, T.; Johnson, J. E.; Mattoussi, H. *Langmuir* **2005**, *21*, 5501.
(31) Raja, K. S.; Wang, Q.; Gonzalez, M.; Manchester, M.; Johnson, J. E.; Finn, M. G. *Biomacromolecules* **2003**, *4*, 472.
(32) Sen Gupta, S.; Raja, K. S.; Kaltgrad, E.; Strable, E.; Finn, M. G. *Chem. Commun.* **2005**, 4315.
(33) Strable, E.; Johnson, J. E.; Finn, M. G. *Nano Lett.* **2004**, *4*, 1385.
(34) Chatterji, A.; Ochoa, W.; Shamieh, L.; Salakian, S. P.; Wong, S. M.; Clinton, G.; Ghosh, P.; Lin, T.; Johnson, J. E. *Bioconjugate Chem.* **2004**, *15*, 807.
(35) Chatterji, A.; Burns, L. L.; Taylor, S. S.; Lomonossoff, G. P.; Johnson, J. E.; Lin, T.; Porta, C. *Intervirology* **2002**, *45*, 362.
(36) Sapsford, K. E.; Soto, C. M.; Blum, A. S.; Chatterji, A.; Lin, T. W.; Johnson, J. E.; Ligler, F. S.; Ratna, B. R. *Biosens. Bioelectron.* **2006**, *21*, 1668.
(37) Raja, K. S.; Wang, Q.; Finn, M. G. *ChemBioChem* **2003**, *4*, 1348.
(38) Gillitzer, E.; Willits, D.; Young, M.; Douglas, T. *Chem. Commun.* **2002**, 2390.
(39) Taylor, D.; Wang, Q.; Bothner, B.; Natarajan, P.; Finn, M. G.; Johnson, J. E. *Chem. Commun.* **2003**, 2770.
(40) Schlick, T. L.; Ding, Z.; Kovacs, E. W.; Francis, M. B. *J. Am. Chem. Soc.* **2005**, *127*, 3718.
(41) Hooker, J. M.; Kovacs, E. W.; Francis, M. B. *J. Am. Chem. Soc.* **2004**, *126*, 3718.
(42) Wang, Q.; Chan, T.; Hilgraf, R.; Fokin, V. V.; Sharpless, K. B.; Finn, M. G. *J. Am. Chem. Soc.* **2003**, *125*, 3192.
(43) Sen Gupta, S.; Kuzelka, J.; Singh, P.; Lewis, W. G.; Manchester, M.; Finn, M. G. *Bioconjugate Chem.* **2005**, *16*, 1572.
(44) Soto, C. M.; Blum, A. S.; Vora, G. J.; Lebedev, N.; Meador, C. E.; Won, A. P.; Chatterji, A.; Johnson, J. E.; Ratna, B. R. *J. Am. Chem. Soc.* **2006**, *128*, 5184.
(45) Klug, A.; Finch, J. T.; Franklin, R. E. *Nature* **1957**, *179*, 683.
(46) Canady, M. A.; Larson, S. B.; Day, J.; McPherson, A. *Nat. Struct. Biol.* **1996**, *3*, 771.
(47) Reddy, V. S.; Natarajan, P.; Okerberg, B.; Li, K.; Damodaran, K. V.; Morton, R. T.; Brooks, C. L., III; Johnson, J. E. *J. Virol.* **2001**, *75*, 11943.
(48) Brenner, S.; Horne, R. W. *Biochim. Biophys. Acta* **1959**, *34*, 103.
(49) Leimkühler, M.; Goldbeck, A.; Lechner, M. D.; Adrian, M.; Michels, B.; Witz, J. *Arch. Virol.* **2001**, *146*, 653.
(50) Kaper, J. M. *Biochemistry* **1964**, *3*, 486.
(51) Katouzian-Safadi, M.; Favre, A.; Haenni, A. L. *Eur. J. Biochem.* **1980**, *112*, 479.
(52) Weibel, N.; Charbonnière, L. J.; Guardigli, M.; Roda, A.; Ziessel, R. *J. Am. Chem. Soc.* **2004**, *126*, 4888.
(53) Hildebrandt, N.; Charbonnière, L. J.; Beck, M.; Ziessel, R. F.; Löhmannsröben, H. G. *Angew. Chem., Int. Ed.* **2005**, *44*, 7612.

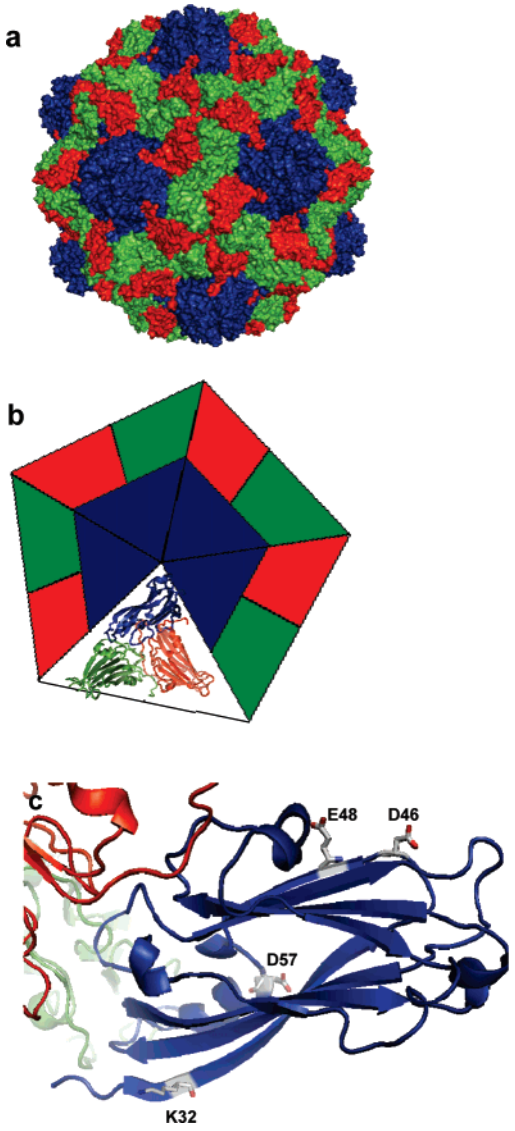

Figure 1. (a) Structure of TYMV capsid with subunits colored blue (chain A), red (chain B), and green (chain C). The chemically identical subunit has a molecular weight around 20 kDa. (b) A pentameric unit of the TYMV capsid with an asymmetric unit presented as a ribbon diagram based on the X-ray crystallography. (c) An enlarged ribbon diagram representation of chain A showing reactive lysine residues and possible reactive carboxylic acid residues (refs 46 and 47).

labeled avidin was used to study the nature of the particle and the protein binding between avidin and biotinylated TYMV. We therefore demonstrated several features of this system not seen before with other bionanoparticle systems. First, communication on the surface of the bionanoparticle between the two reactive sites was easily realized via FRET. Second, the protein binding ability of a substrate was not perturbed upon conjugation to the bionanoparticle. Third, the luminescence behavior of the lanthanide metal complex was nearly identical both conjugated and unconjugated to the bionanoparticle. These features have implications in the application of TYMV in sensing, protein binding studies, and even photovoltaic and electronics owing to the communication on the surface of the particle.

(54) Charbonnière, L.; Ziessel, R.; Guardigli, M.; Roda, A.; Sabbatini, N.; Cesario, M. *J. Am. Chem. Soc.* **2001**, *123*, 2436.

2. Experimental Procedures

General. Most bioreagents were purchased from Bio-Rad or Fisher and used without further purification. Anti-TYMV antibody was received as a gift from Professor Theo Dreher. Reactive dyes were purchased from Molecular Probes and used without further purification. Unless otherwise indicated, "buffer" refers to 10 mM potassium phosphate at pH 7.8. Size exclusion columns for purification of virus-containing reaction mixtures were prepared by preswelling 23 g of Bio-Gel P-100 (Bio-Rad) in 400 mL of buffer and loading the gel into Bio-Spin disposable chromatography columns (Bio-Rad). The columns were allowed to drain upon standing and were then further dried by centrifugation (3 min at 800*g*). For 80 μL of virus solution (1 mg/mL), approximately 1 mL of prepared gel is required. Ultracentrifugation was performed at the indicated rpm values using a Beckman Optima L-90K ultracentrifuge equipped with either SW41 or 50.2 Ti rotors. TEM analyses were carried out by depositing 20 μL aliquots of each sample at a concentration of 0.1−0.3 mg/mL onto 100 mesh carbon-coated copper grids for 2 min. The grids were then stained with 20 μL of 2% uranyl acetate and viewed with a Hitachi H-8000 TEM electron microscope. FPLC analyses were performed on an AKTA Explorer (GE Biotech) using a Superose-6 size exclusion column. Potassium phosphate buffer (0.05 M, pH 7.0) with 0.15 M NaCl was used as eluent, and the intact virions show retention volume of approximately 10 mL at an elution rate of 0.4 mL/min, whereas broken particles and individual subunit proteins elute after more than 20 mL. Western blot analysis was carried out using a Bio-Rad Mini Trans-Blot electrophoretic transfer cell with a 15% polyacrylamide gel.

Purification of TYMV. Chinese cabbage was grown for 3 weeks after which it was inoculated with TYMV. After 1 week leaves began showing symptoms. After an additional 2 weeks, the leaves were picked and subjected to purification. Infected leaves were blended with 3× volume of buffer and 0.1% β-mercaptoethanol. The mixture was filtered, and the filtrate was subjected to centrifugation to remove bulk plant material. The supernatant was collected and clarified by adding an equal volume of $CHCl_3$/1-butanol (v/v = 1:1). The aqueous layer was collected, and the virus was precipitated with 8% PEG 8K and 0.2 M NaCl. The pellet was centrifuged, resuspended in buffer, and purified by centrifuging over a sucrose gradient which showed two bands, one for the filled particle and one for the empty particle. In general, the virus was stored in buffer at a concentration of 10 mg/mL at 4 °C and was stable for months.

SDS−PAGE Analysis. Polyacrylamide gel electrophoresis was carried out in a Bio-Rad MiniPROTEAN 3 gel electrophoresis cell. For analysis by coomassie blue staining, 1 μg of TYMV was denatured by heating at 95 °C for 5 min with Tris−HCl buffer containing β-mercaptoethanol, bromophenol blue, and glycerol. The proteins were then resolved on a 15% polyacrylamide gel at 200 V for 1 h and stained with Bio-Rad Biosafe coomassie blue stain for 1 h and destained with distilled water. Fluorescently labeled TYMV was visualized with a UVP Epi Chemi II imager before staining.

MALDI-TOF MS of TYMV Subunit. A solution of TYMV (1 mg/mL, 26 μL) was treated with guanidinium−HCl (6.0 M, 4 μL) for 5 min at room temperature. The denatured protein was spotted onto a MALDI plate using Millipore $ZipTip_{\mu\text{-}C18}$ tips to remove the salts. The samples were analyzed using a Bruker Ultraflex TOF/TOF mass spectrometer with MS-grade sinapinic acid in 70% acetonitrile and 0.1% TFA as the matrix.

Trypsin In-Gel Digestion and MALDI Study. Pure viral protein (1 mg) was resuspended in Tris buffer (100 mM, 26 μL). Urea (6.0 M, 100 μL) and DTT (200 mM, 5 μL) were added, and the solution was incubated for 1 h at room temperature. Then the solution was diluted 10 times and incubated with sequence-grade modified trypsin (protein/enzyme = 50:1) for 18 h at 37 °C. The pH was then adjusted to slightly below 6 to quench the reaction. Tryptic digests were then analyzed by MALDI-TOF MS and MALDI-TOF−TOF MS/MS using a Bruker

Scheme 1

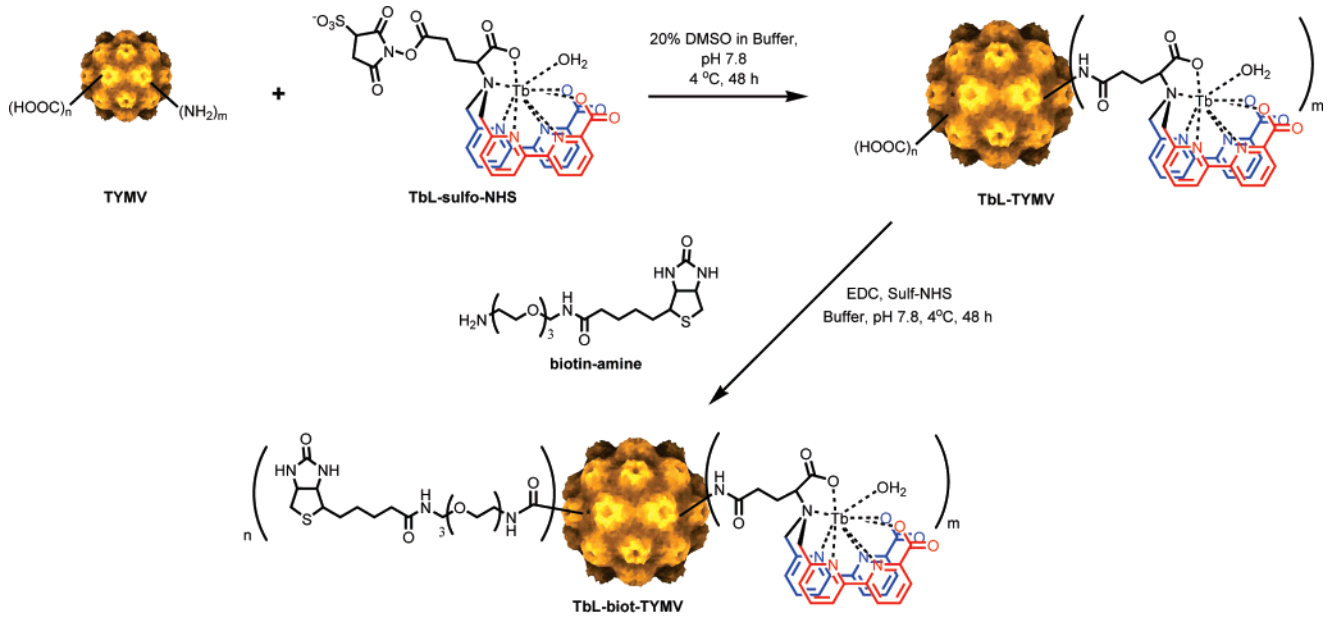

Ultraflex TOF/TOF mass spectrometry and mass spectroscopy grade α-hydroxycinnaminic acid in 70% acetonitrile and 0.1% TFA as the matrix.

Dual Modification of WT TYMV. The terbium complex in its activated sulfo-NHS ester form (Tb**L**) was synthesized according to previously published procedures.[52,53] Reactions with TYMV were carried out at a concentration of 1 mg/mL of virus and 100 mol equiv of Tb**L** in 20% DMSO and 80% buffer for 24 h and purified by either ultracentrifugation over a sucrose gradient or by size exclusion chromatography as described above. Each reaction was analyzed by UV−vis spectroscopy, TEM, FPLC, SDS−PAGE, and fluorescence spectroscopy. Subsequent modification with biotin was carried out by incubating TYMV at 1 mg/mL with biotin-amine (5 mM) catalyzed with EDC and sulfo-NHS in potassium phosphate buffer at pH 7.8, to give dual-modified TYMV, Tb**L**−Biot−TYMV. Total recovery yield of the viral particles after dual modification was around 25%. The Tb**L**−Biot−TYMV was analyzed by UV−vis spectroscopy, TEM, FPLC, SDS−PAGE, Western blot, and fluorescence spectroscopy.

Spectroscopic Analysis. Absorption spectra were recorded on an Uvikon-933 spectrometer. Steady-state and time-resolved luminescence spectra were recorded independently on a Perkin-Elmer LS50 or a PTI Quantamaster spectrofluorimeter. Luminescence quantum yields were determined on the Perkin-Elmer LS50 spectrometer in the phosphorescence mode using a 0 μs delay time and 10 ms integration windows. Absolute quantum yield Φ for the luminescence of Tb upon ligand excitation was given by $\Phi_x = \Phi_{ref}(I_x od_{ref})/(I_{ref} od_x)$,[55] where x and ref refer to the sample and the reference, respectively, and I and od stand for the total emission intensity and the optical density of the sample at the excitation wavelength. Tb**L** in water was taken as the reference (Φ = 31%),[52] using samples with absorbance values not exceeding 0.05 at the excitation wavelength. Excitation was performed at 308 nm unless otherwise stated, and if necessary, wavelength dependence of the excitation intensity was corrected. The estimated relative error on Φ_x is 15%. Terbium luminescence lifetimes were determined on the PTI QuantaMaster spectrometer by measuring the temporal intensity decay at the maximum of emission (545 nm, $^5D_4 \rightarrow {}^7F_5$ transition of Tb) upon ligand excitation, over at least five lifetime periods decomposed in 400 canals, or at 485 nm (high-energy tail of the $^5D_4 \rightarrow {}^7F_6$ transition) during RET titration experiments, to avoid residual signal from the acceptor molecule. The decays were fitted with mono- and biexponential decays with the software implemented by the supplier.

(55) Haas, Y.; Stein, G. *J. Phys. Chem.* **1971**, *75*, 2697.

Resonance Energy Transfer Experiments. In a typical experiment, a 2 mL solution of the dual-labeled Tb**L**−Biot−TYMV samples (concentration from 7 to 100 pM) in 0.01 M potassium phosphate buffer (pH 7.8) was titrated by increasing amounts of AlexaFluor488−avidin (Molecular Probes) in the same buffer. After each aliquots addition the UV−vis spectra of the solution was recorded to calculate the AlexaFluor488−avidin content assuming a labeling ratio of three AlexaFluor488 dyes per avidin protein as given by the producer. Time-resolved emission spectra were recorded on both Perkin-Elmer LS50 and PTI Quantamaster spectrofluorimeters, upon excitation at 308 and 320 nm with delays varying from 70 to 150 μs depending on the apparatus used. The luminescence lifetime of terbium was obtained by measuring the luminescence decay curve at 485 nm ($^5D_4 \rightarrow {}^7F_6$ transition) and, when intense enough, that of the AlexaFluor488 acceptor at 523 nm. Short fluorescence of AlexaFluor488 was also measured upon excitation of the fluorophore at 450 nm to discard possible interference due to direct excitation of the acceptor. The intensity ratio for emission of the acceptor (I_{523}) over emission of the donor (I_{485}) was calculated and plotted versus the amount of added avidin.

3. Results

Dual Modification of TYMV. There are six total lysine residues on a subunit of TYMV; however, only K32 can be selectively addressed with *N*-hydroxysuccinimide (NHS) reagents as shown by detailed proteomics studies.[56] When using fluorescent dyes to monitor the reaction, up to 60 dye molecules could be conjugated to TYMV via the amidation of K32. Within each asymmetric unit of TYMV capsid, there are three different subunits chains termed A, B, and C as shown in different colors in Figure 1. Although they are chemically identical proteins, each subunit is located in a different microenvironment and adapts a slightly different configuration. While chains B and C make up hexameric structures on the virus, chain A makes up the pentameric units. Studies on the crystal structure of TYMV have shown that chain A is much more flexible compared to B and C, especially at the N-terminal region where the Lys-32 located.[57,58] It is possible that the flexible A chain contains our

(56) Barnhill, H. N.; Reuther, R.; Ferguson, P. L.; Dreher, T.; Wang, Q. *Bioconjugate Chem.* **2007**, *18*, 852.
(57) van Roon, A. M.; Bink, H. H.; Plaisier, J. R.; Pleij, C. W.; Abrahams, J. P.; Pannu, N. S. *J. Mol. Biol.* **2004**, *341*, 1205.

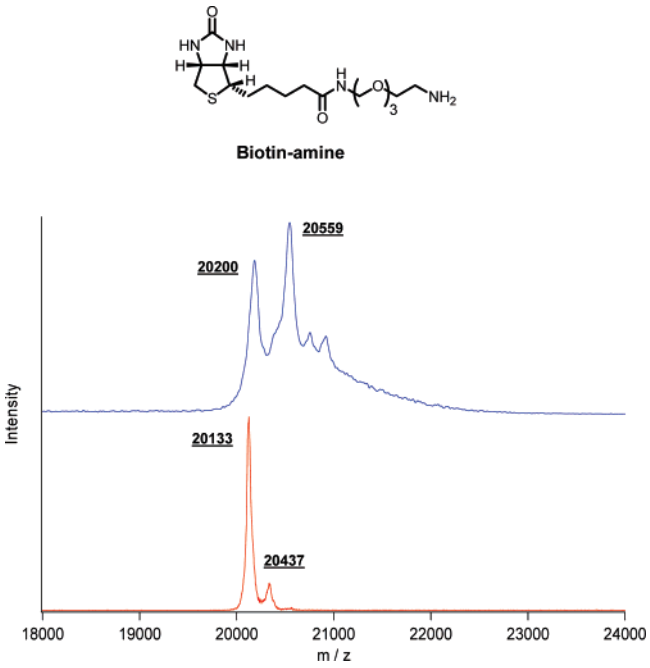

Figure 2. Comparison of whole protein MALDI-TOF MS of native TYMV protein (red) and biotin−TYMV (blue). Wild-type TYMV (20 133 *m*/*z*) was used as external standard. The difference in mass was consistent to the attachment of a biotin motif. Smaller peaks indicate matrix adducts.

reactive site; therefore, only about one-third of the Lys-32 are chemically addressable, which gave a total loading of 60. However, due to the large size of the Tb**L** complex and its low solubility, it is more probable to have a partial loading of approximately 40 per particle according to previous reactivity studies.[56]

Similar as reported,[38,40,59] the reactivity of carboxyl groups was tested with amines under activation with 1-(3-dimethylaminopropyl-3-ethylcarbodiimide) hydrochloride (EDC) and sulfo-NHS, which revealed that approximately 90 carboxylic groups could be modified, and up to 120 under forcing conditions.[56] Tryptic digestion and sequential MS analysis indicated activation of the carboxyl groups at the most exposed part of the β-barrel (between D46 and D57) on the exterior surface. Because the peptide has three amino acid residues with carboxyl groups, i.e., D46, E48, and D57, it remains as an ongoing effort to identify the location of reactive carboxyl residues with MS/MS studies. In order to test the ability of protein binding, we chose the biotin (shown also in Scheme 1) as a prototype ligand. Upon overnight incubation of TYMV with biotin-amine, catalyzed with EDC and sulfo-NHS in a potassium phosphate buffer (pH 7.8), TYMV was successfully derivatized. MALDI-TOF MS analysis showed the molecular weight increase corresponding to the attachment of biotin motifs (Figure 2). According to the MALDI MS, about 60% of the subunits were biotinylated, which is consistent with our previous study.[56]

With the use of lysine K32 and reactive carboxyl groups, two distinctive functionalities could be anchored on TYMV as shown in Scheme 1. Biotin was used as the recognition unit and the terbium complex as the signaling unit due to the unique

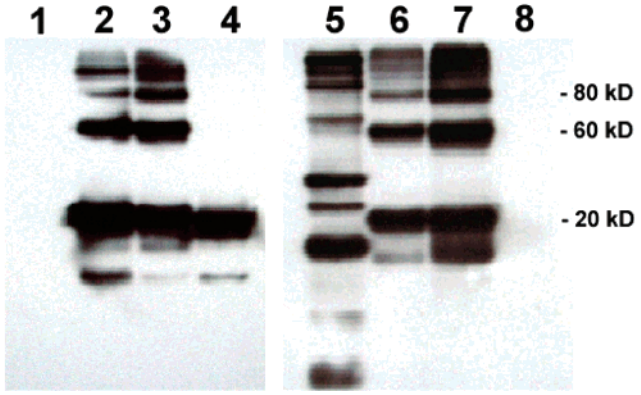

Figure 3. Western blot analysis of dual-modified TYMV with anti-TYMV antibodies (lanes 1−4) and avidin−horseradish peroxidase (lanes 5−8): lanes 1 and 5, biotin standard from Bio-Rad; lanes 2 and 6, Tb**L**−Biot−TYMV; lanes 3 and 7, biotin-derivatized TYMV; lanes 4 and 8, wild-type TYMV.

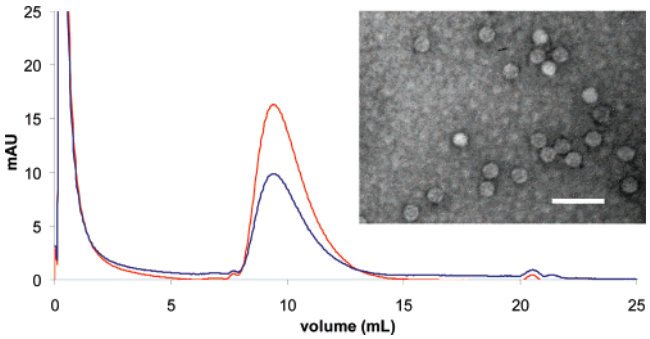

Figure 4. FPLC showing intact virus eluting at 10 mL and A_{260} nm (red) and A_{280} nm (blue) over a size exclusion column. The inset shows TEM images of dual-modified particles. Scale bar = 100 nm.

fluorescent properties.[52,54,60] First, the sulfo-NHS ester of the terbium complex Tb**L** was conjugated to the K32 of TYMV to give Tb**L**−TYMV. An EDC-mediated coupling reaction was then performed to add biotin groups on TYMV and afford dual-modified Tb**L**−Biot−TYMV. Anti-TYMV antibodies and avidin−horseradish peroxidase were utilized in the Western blot analysis of Tb**L**−Biot−TYMV, which showed that biotin was successfully conjugated to the virus and specifically bound the tetrameric protein avidin (Figure 3). Total recovery of the particle after dual modification was about 25%. The presence of higher molecular weight bands could be observed with biotinylated TYMV caused by intramolecular cross-linking of the coat proteins, which would not impact on the integrity of the dual-modified particle as confirmed by size exclusion fast processing liquid chromatography (FPLC) and transmission electron microscopy (TEM) (Figure 4). Circular dichroism spectra were taken for TYMV before and after modification. However, signals from the viral scaffold overshadowed other potential signals from newly attached functional groups (see the Supporting Information).

Photophysical Characterization of Dual-Modified TYMV. The spectroscopic properties of the different TYMV samples were studied by means of absorption and luminescence spectroscopy. The maximum of absorption of wild-type (WT) TYMV appeared at 260 nm, corresponding to the absorption

(58) Larson, S. B.; Lucas, R. W.; Greenwood, A.; McPherson, A. *Virology* **2005**, *334*, 245.
(59) Steinmetz, N. F.; Lomonossoff, G. P.; Evans, D. J. *Langmuir* **2006**, *22*, 3488.
(60) Basu, G.; Allen, M.; Willits, D.; Young, M.; Douglas, T. *J. Biol. Inorg. Chem.* **2003**, *8*, 721.

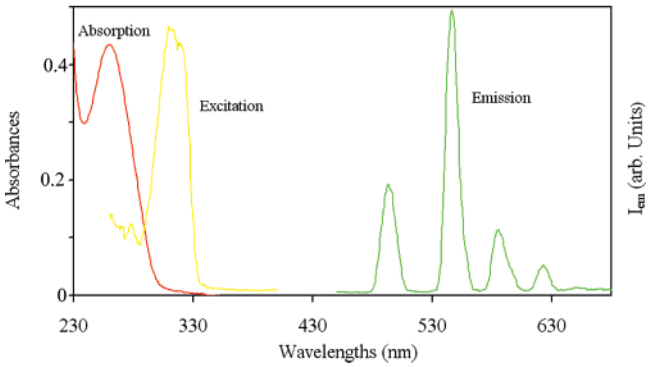

Figure 5. UV−vis absorption (red), excitation (λ_{em} = 545 nm, yellow), and fluorescent emission (λ_{exc} = 320 nm, cutoff filter at 390 nm, green) spectra of Tb**L**−TYMV at a concentration of 9.5 nmol·L^{-1} in 0.1 M KPO_4 buffer, pH = 7.8.

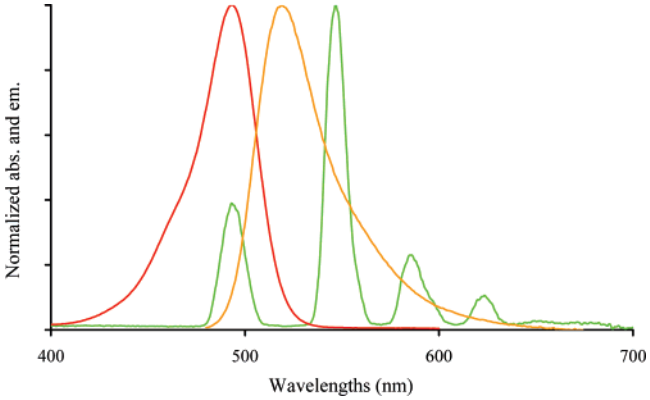

Figure 6. Normalized absorption spectrum of A488−avidin (red) and emission spectra of A488−avidin (orange) and of the dual-labeled Tb**L**−Biot−TYMV (green) in 0.1 M potassium phosphate buffer at pH 7.8.

of the nucleotides constituting the RNA. The emission spectra displayed one main emission band with a maximum at 340 nm. Upon emission at 340 nm, the excitation spectrum revealed a maximum of excitation at 283 nm, different from the maximum of absorption (260 nm). This points to emission arising mainly from the amino acids residues of the protein shell (the aromatic groups of tyrosine and tryptophan having maximum of absorption at ca. 280 nm), rather than from the nucleotide bases constituting the RNA strand.

The absorption spectrum of Tb**L**−TYMV showed almost identical features as that of WT TYMV, with a maximum absorption at 260 nm (Figure 5). Unfortunately, the absorption corresponding to the Tb**L** complex itself is beneath in the low-energy tail of the spectrum and cannot be extracted from this spectrum prohibiting the possibility to calculate the labeling ratio on the basis of UV−vis spectrum deconvolution. Upon excitation below 290 nm, the emission spectrum displayed the same emission bands as the native virus. At higher wavelengths, the characteristic emission bands of Tb were observed evidently (Figure 5) with a mixture of virus residual fluorescence.

This spurious signal disappeared as soon as a 30 μs delay time was inserted between pulsed excitation and emission intensity measurement. Measuring the Tb-centered emission revealed a maximum of excitation at 310−320 nm, which is typical for the excitation spectrum of the lanthanide complexed bipyridyl-carboxylate strands of Tb**L**,[52,61] arising from a ligand to metal energy transfer, the so-called antenna effect.[62,63] The luminescence decay of the Tb emission was perfectly fitted with single-exponential behavior, pointing to the labeling of complexes located at very similar environments all over the capsid structure. The luminescence lifetime of terbium labels on TYMV in buffered solution was 1.52 ± 0.02 ms, slightly larger than that measured for Tb**L** in pure water (1.48 ms),[52] but very similar to the one measured for Tb**L** in the 0.1 M phosphate buffer at pH 7.8 (1.50 ± 0.02 ms), which indicated the possible effect of phosphate anions.[64] As no evident difference has been observed between the UV−vis absorption spectra of Tb**L** in pure water or in the phosphate buffer, the impact of phosphate anions is attributed to a decrease of the nonradiative deactivation pathways that quench the Tb excited state and resulted in an increase of the metal-centered luminescence quantum yield, Φ_{Ln}, rather than in an increased sensitization process, η_{sens}. The absolute overall luminescence quantum yield upon ligand excitation at 308 nm, $\Phi_{Ov} = \Phi_{Ln}\eta_{sens}$, was determined to be 11% relative to Tb**L** in water. Interestingly, this value is far smaller than that of pure Tb**L**, despite an increased luminescence lifetime. This may be due to the fact that much of the photons absorbed at 308 nm, are absorbed by the TYMV and not available for ligand excitation and therefore Tb emission.

The absorption spectrum of the dual-labeled Tb**L**−Biot−TYMV is also dominated by the intense absorption bands of TYMV at 260 nm. Emission and excitation are very similar to that observed for Tb**L**−TYMV, displaying residual virus fluorescence and Tb luminescence upon ligand-centered excitation. The Tb luminescence lifetime can be perfectly fitted with a single-exponential behavior, but the luminescence lifetimes shifted slightly to 1.62 ms. When excited at 320 nm, the luminescence quantum yield increased up to 37% which was in good agreement with the value expected on the basis of the increase of luminescence lifetime (34% for a 1.62 μs lifetime).[52] These findings suggest that the luminescence behavior of Tb**L** conjugated to TYMV is not perturbed compared to that of free Tb**L**, a previously undemonstrated property with nanoparticle systems.

Resonance Energy Transfer Studies. In order to show a possible communication between the two reactive residues, dual-modified TYMV was used as an energy donor in the frame of a time-resolved fluoroimmuno assay (TRFIA), in which avidin labeled with AlexaFluor488 (A488) was used as an energy acceptor. TRFIA is based on a dual-intensity measurement at two different wavelengths, requiring no internal calibration, and is independent of the concentration of the samples. Providing that the energy donor and acceptor are brought in close spatial proximity and that their respective emission and absorption spectrum display significant overlapping, excitation through the donor leads to a RET which can be measured by the observation of a long-lived acceptor emission. As shown in Figure 6, the absorption spectrum of A488 overlaps substantially with the fluorescence spectra of Tb**L**, which makes it a good fluorophore for our study. An obvious advantage of using such long-lived labels as energy donors resulted from the apparent increase of

(61) Comby, S.; Imbert, D.; Chauvin, A. S.; Bunzli, J. C.; Charbonnière, L. J.; Ziessel, R. F. *Inorg. Chem.* **2004**, *43*, 7369.
(62) Weissmann, S. I. *J. Chem. Phys.* **1942**, *10*, 214.
(63) Sabbatini, N.; Guardigli, M.; Lehn, J.-M. *Coord. Chem. Rev.* **1993**, *123*, 201.
(64) Charbonnière, L. J.; Schurhammer, R.; Mameri, S.; Wipff, G.; Ziessel, R. F. *Inorg. Chem.* **2005**, *44*, 7151.

the acceptor lifetime.[65] When fluorescent dyes such as A488 are used as energy acceptors, their luminescent lifetimes can be increased from few nanoseconds in the unbound state up to few hundreds of microseconds when the energy transfer takes place from the Ln energy donors.[65,66] It allows the integration of luminescence spectra in the time-resolved mode, thereby allowing for elimination of the spurious fluorescence of the sample, especially that due to direct excitation of the acceptor. Time-resolved acquisition can also eliminate the artifacts resulting from light scattering in the apparatus and afford a large increase in the detection sensitivity.[54,67]

On the basis of these spectroscopic data, eq 1 allows for the calculation of the Förster's critical radius, R_0, the distance at which the resonant energy transfer and the spontaneous decay of the acceptor are equally probable.[68]

$$R_0 = 0.2108[\kappa^2 \Phi_{Tb}/n^4 \int I_D(\lambda)\epsilon_A(\lambda)\lambda^4 \, d\lambda]^{1/6} \qquad (1)$$

In eq 1, Φ_{Tb} refers to the metal-centered luminescence quantum yield,[65] n is the refractive index of the medium, $I_D(\lambda)$ is the normalized fluorescence intensity of the donor, $\epsilon_A(\lambda)$ is the molar absorption coefficient of the acceptor, and κ^2 is the orientational factor. It is assumed that the use of a donor with a long lifetime of the excited state leads to random distribution of the donor and acceptor dipoles and that a value of $^2/_3$, resulting from an average isotropic distribution, can be used for κ^2.[65] On the basis of literature data on luminescence lifetimes of Tb**L**,[52,67] and using the measured lifetime in the experimental conditions, the metal-centered luminescence quantum yield can be estimated according to reported theoretical procedure,[67] giving a value of 54% (see the Supporting Information for full calculation details). With the use of a refractive index of 1.4 for proteins in aqueous solvents,[69] the Förster radius was calculated to be 41 ± 2 Å. This radius is in a common range for donor−acceptor couples[68] but should be largely increased by the use of an acceptor absorbing at longer wavelengths such as tetramethylrhodamine, the absorption of which would overlap with the emission arising from $^5D_4 \rightarrow {}^7F_J$ ($J = 3-5$) transitions of Tb at 545, 590, and 615 nm.

The availability of RET from terbium to the A488 was checked by titration experiments, in which increasing amounts of labeled avidin was added to solutions of the dual-labeled virions in 0.01 M potassium phosphate at pH 7.8. Time-resolved emission spectra were recorded showing the emergence of a new long-lived emission signal with a maximum at 523 nm, concomitant with the addition of avidin, and attributed to the sensitized emission of A488 (see the inset in Figure 7). From these spectra, the delayed emission intensities at 495 nm (Tb) and 523 nm (Alexa Fluor 488) were collected, and their ratio, $R = I_{523}/I_{495}$, was measured and normalized at $R = 1$ for no avidin added. Figure 7 shows the evolution of R as a function of added avidin. The possibility of residual fluorescence of A488 due to direct excitation was ruled out by control experiments with excitation in the absorption band of the acceptor at 450 nm. In all cases,

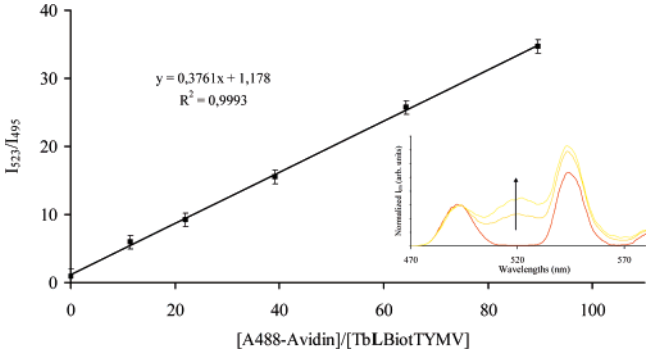

Figure 7. Evolution of the normalized delayed intensity ratio $R = I_{523}/I_{495}$ as a function of equiv of A488−avidin ([TYMV] = 10.6 nmol·L^{-1}) added to a solution of dual-labeled Tb**L**−Biot−TYMV. Points on the calibration curve correspond to 0, 11.4, 21.8, 38.9, 63.9, and 89.0 molar equiv of avidin per TYMV. Inset: Normalized delayed luminescence spectra (λ_{exc} = 308 nm, delay = 150 μs) of the dual-labeled TYMV sample containing 0 (red), 63.9 (orange), and 89.0 (yellow) molar equiv of A488−avidin, showing the increase in time-resolved emission signal at 523 nm.

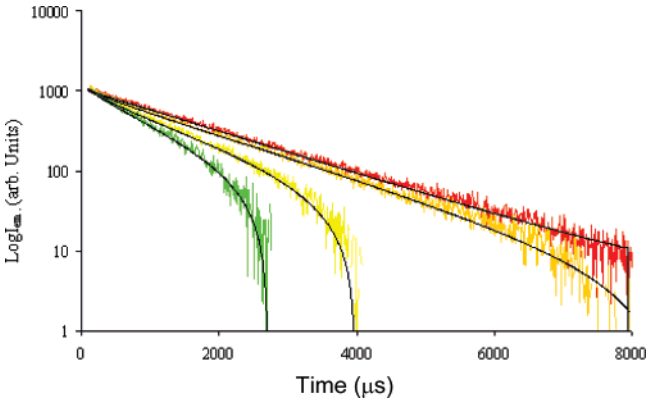

Figure 8. Evolution of the Tb-centered emission (λ_{exc} = 308 nm, λ_{em} = 495 nm) of Tb−Biot−TYMV in the presence of 0 (red), 21.8 (orange), 38.9 (yellow), and 89.0 (green) equiv of A488−avidin.

imposition of the delay time led to the vanishing of fluorescence as was further evidenced by intensity decay profiles for emission at 523 nm upon visible excitation at 450 nm. Although the solutions were rather diluted, it was also important to eliminate the possibility of dynamic RET and that of RET due to nonspecific binding interactions of TYMV with avidin. This was achieved by similar experiments measuring the time-resolved emission spectra of solutions of Tb**L**−TYMV (concentration of TYMV = 5.45 nmol·L^{-1}) containing A488-labeled avidin (0−23 equiv). No sensitization of A488 could be observed in the time-resolved emission spectra upon excitation of Tb**L** at 308 nm, confirming that the RET was due to the spatial proximity afforded by the strong biotin−avidin interaction. For large amounts of avidin (more than 90 equiv), the solution became turbid and a pale yellow precipitate appeared in the solution, probably the result of the insolubility of the heavy aggregates formed by TYMV and avidin molecules.

As expected on the basis of an energy transfer phenomenon, the average luminescence lifetime of the terbium decreases during the titration. Figure 8 displays the evolution of the terbium decay profiles at varying points of the titration, together with their biexponential fitting functions. While in the absence of acceptor the lifetime can be perfectly fitted with a single exponential with 1.62 ms lifetime in our case, the presence of acceptor led to more complex behaviors which can only

(65) Selvin, P. R.; Hearst, J. E. *Proc. Natl. Acad. Sci. U.S.A.* **1994**, *91*, 10024.
(66) Cha, A.; Snyder, G. E.; Selvin, P. R.; Bezanilla, F. *Nature* **1999**, *402*, 809.
(67) Charbonnière, L. J.; Hildebrandt, N.; Ziessel, R.; Löhmannsröben, H.-G. *J. Am. Chem. Soc.* **2006**, *128*, 12800.
(68) Valeur, B. *Molecular Fluorescence, Principles and Applications*; Wiley-VCH: Weinheim, Germany, 2002.
(69) Lakowicz, J. R. *Principles of Fluorescence Spectroscopy*; Kluwer Academic/Plenum Publishers: New York, 1999.

Table 1. Evolution of the Relative Percentages of Nontransferring (NT) and Transferring (T) Terbium Species and Lifetimes of the Sensitized Acceptor (τ_{AD}) with the Corresponding Energy Transfer Efficiencies (η_{eff}) and Average Donor−Acceptor Distance (r)

[avidin]/[TYMV]	% of NT	% of T	τ_{AD}	η_{eff}	r
0	100	0			
21.8	84	16	497 ± 15	0.69	35.9
38.9	74	26	542 ± 15	0.66	36.6
63.9	60	40	568 ± 16	0.65	37.0
89.0	55	45	496 ± 10	0.69	35.8

conveniently be fitted with at least two exponential components. Assuming that the Tb populations were composed from species not subject to transfer (with lifetime τ_D) and species which transfer (with lifetimes τ_{DA}), the biexponential fitting procedure was conducted using the lifetime of Tb only (1.62 ms) for τ_D, while that of transferring species was fitted in the process. Pre-exponential factors gave an evaluation of the relative amounts of each population. Table 1 summarizes values obtained for the relative amounts of each species.

In parallel, the A488 acceptor lifetime increases as soon as the energy transfer took place. Assuming that the lifetime of the free acceptor is very short, compared to the lifetime of the donor in the presence of the acceptor, the long-lived tail lifetime of the acceptor in the presence of the donor τ_{AD} equals τ_{DA}, the lifetime of the donor transferring energy.[68] Fitting of the long-lived tail of the acceptor was conveniently realized with single-exponential decay functions resulting in τ_{AD} (or τ_{DA}) values presented in Table 1. From there, the energy transfer efficiency η_{eff} and average donor−acceptor distances r were calculated with the eqs 2 and 3, where R_0 is the calculated Förster radius (41 Å).

$$\eta_{eff} = 1 - \tau_{DA}/\tau_D \quad (2)$$

$$r = (1/\eta_{eff} - 1)^{1/6} R_0 \quad (3)$$

Results showed that the energy transfer process is relatively homogeneous during the titration with an average efficiency of 67% ± 2 % leading to an average donor acceptor distance of 36.3 ± 0.8 Å.

With the use of the calibration curves obtained from Figure 7, a detection limit of 23 nmol·L^{-1} of avidin was calculated on the basis of a minimal measurable signal larger than 3 times the standard deviation ($I_{min} > 3\sigma(I)$). It is worth pointing out that this result was obtained with routine fluorimeter and that dedicated instruments using high-power excitation sources (lasers) and specific filter sets could lead to improvement of 2−3 orders of magnitude in the detection limit,[66] affording a picomolar sensitivity.

On the basis of the proteomic analysis of the labeled TYMV, the fluorophore-labeled residue was clearly established as being the K32 lysine residue. Nevertheless, it has not been possible to ascertain exactly the origin of the biotinylated residue between D46, D57, and E48. Additionally, it should be kept in mind that the RET distance is between the Tb**L** donor at K32 on TYMV and the AlexaFluor dye on the avidin protein, which does not reflect the relative position of K32 and the carboxyl residues on the surface of TYMV. Because the biotin-amine used in this study has a long flexible chain and the large size of the avidin molecule, the donor and acceptor distances could not be determined easily. However, our RET studies showed that the small differences in τ_{DA} values can hardly be distinguished in the mathematical analysis of the luminescence decay. The use of an averaged τ_{DA} value weighted by the efficiencies of each process afforded a lifetime of 582 μs, which falls in the range of measured values, within experimental errors, as did the corresponding averaged energy transfer efficiency (64%). This result showed that the RET took place within a single environment and suggested the biotinylation reaction located at one of the carboxyl residues.

4. Conclusions

The icosahedral plant virus TYMV was selected as a prototype bionanoparticle for the TRFIA. On the basis of orthogonal chemical reactions, TYMV was labeled with luminescent terbium complexes and biotin motifs, which allows for use of this nanoparticle as a scaffold in TRFIA, using fluorescently labeled avidin as the energy acceptor. Detailed RET studies have shown (1) the protein binding properties of small molecules were not adversely affected by conjugation to TYMV, (2) the luminescence properties of Tb**L** that bound to TYMV were nearly identical to that of free Tb**L**, and (3) there was clear communication between the two fixed reactive sites on the surface of the particle. These properties demonstrate that dual-labeled bionanoparticles can serve as a scaffold for future TRFIA in cell binding studies. The improvement of the donor−acceptor spectral overlap should greatly improve the efficiency of energy transfer, and using more a dedicated instrument may easily give a picomolar level detection sensitivity. This result paves the way for other possible bionanoparticle-based nanosensors using different recognition events. Moreover, the communication present on the surface of the bionanoparticle may lead to other applications in electronics and photochemistry.

Acknowledgment. This work was partially supported by the USA NSF−NER program, DOD−DURIP, and the W. M. Keck Foundation, and the French Centre National de la Recherche Scientifique and Ministère de la Recherche et de l'Education. We are grateful to Professor Alex McPherson for the TYMV inoculums, Professor Theo Dreher for the anti-TYMV antibodies, Lisa Alexander and Dr. Venkata S. Subbaiah for the assistance of TYMV production, and L. Andrew Lee for helpful discussion.

Supporting Information Available: Complete ref 6; additional mathematical analyses and CD spectra of virus particles. This material is available free of charge via the Internet at http://pubs.acs.org.

JA069148U